ENDOR Spectroscopy Reveals the 'Free' 5′-deoxyadenosyl Radical in a Radical SAM Enzyme Active Site Actually is Chaperoned by Close Interaction with the Methionine-Bound [4Fe-4S]$^{2+}$ Cluster

Hao Yang,[1] Madeline B. Ho,[1] Maike N. Lundahl,[2] Martin A. Mosquera,[2]
William E. Broderick,[2] Joan B. Broderick,[2]* Brian M. Hoffman,[1]*

[1]Department of Chemistry, Northwestern University, Evanston, Illinois 60208, USA
[2]Department of Chemistry and Biochemistry, Montana State University, Bozeman, Montana 59717, USA

Abstract

$^{1/2}$H and ^{13}C hyperfine coupling constants to 5′-deoxyadenosyl (5′-dAdo•) radical trapped within the active site of the radical *S*-adenosyl-L-methionine (SAM) enzyme, pyruvate formate lyase activating-enzyme (PFL-AE), both in the absence of substrate and the presence of a reactive peptide-model of the PFL substrate, are completely characteristic of a classical organic free radical whose unpaired electron is localized in the 2pπ orbital of the sp^2 C5′-carbon (*J. Am. Chem. Soc.* **2019**, *141*, 12139-12146). However, prior ENDOR measurements had indicated that this 5′-dAdo• free radical is never truly 'free': tight van der Waals contact with its target-partners and active-site residues guide it in carrying out the exquisitely precise, regioselective reactions that are hallmarks of RS enzymes. Here, our understanding of how the active site chaperones 5′-dAdo• is extended through the finding that this *apparently* unexceptional organic free radical has an anomalous g-tensor and exhibits significant ^{57}Fe, ^{13}C, ^{15}N, and ^{2}H hyperfine couplings to the adjacent, isotopically-labelled, methionine-bound [4Fe-4S]$^{2+}$ cluster co-generated with 5′-dAdo• during homolytic cleavage of cluster-bound SAM. The origin of the ^{57}Fe couplings through non-bonded radical-cluster contact is illuminated by a formal exchange-coupling model and BS-DFT computations. Incorporation of ENDOR-derived distances from C5′(dAdo•) to labelled-methionine as structural constraints yields a model for active-site positioning of 5′-dAdo• with short, non-bonded C5′-Fe distance (~ 3Å). This distance involves substantial motion of 5′-dAdo• *towards* the unique Fe of the [4Fe-4S]$^{2+}$ cluster upon S-C(5′) bond-cleavage, plausibly an initial step towards formation of the Fe-C5′ bond of organometallic complex, Ω, the central intermediate in catalysis by radical-SAM enzymes.

Introduction

Radical reactions are central to enzymatic catalysis, and in large part are carried out by the largest enzyme superfamily in Nature, the radical *S*-adenosyl-L-methionine (SAM) enzymes (RS enzymes), with over 700,00 members spanning all kingdoms of life and exhibiting remarkable functional diversity.[1-3] These reactions are initiated through H-atom abstraction from substrate by the 5′-deoxyadenosyl (5′-dAdo•) radical, which is created by reductive cleavage of the S-C5′ bond of SAM upon electron transfer from the $[4Fe\text{-}4S]^{1+}$ cluster, which chelates the amino-acid moiety of SAM.

Strenuous efforts to trap and fully characterize 5′-dAdo• in B12 and RS enzymes were unavailing over decades – the primary C5′ radical was simply too reactive to trap – although an allylic analogue was characterized[4] – until we first captured 5′-dAdo• in an RS enzyme through reductive SAM cleavage initiated by cryogenic photoinduced electron transfer from the $[4Fe\text{-}4S]^{1+}$ cluster to SAM in the absence of substrate.[5] The resulting 5′-dAdo• was definitively identified through the use of isotopically labeled SAM combined with EPR and electron-nuclear double resonance (ENDOR) spectroscopy, and its structure was analyzed using density functional theory (DFT) computations, **Fig 1**.[5] Subsequently the 5′-dAdo• radical was shown to form in diverse RS enzymes upon photoinduced electron transfer from the $[4Fe\text{-}4S]^{1+}$ cluster, while in other RS enzymes a $\bullet CH_3$ radical forms instead. These results led to an understanding of the electronic origin of regioselectivity as a consequence of the Jahn-Teller effect during reductive cleavage of SAM.[6-8] The 5′-dAdo• radical also was freeze-trapped and characterized in the presence of a non-reactive substrate analogue.[9] Most recently, 5′-dAdo• was caught in the act of catalysis during reaction of the RS enzyme pyruvate formate-lyase (PFL) activating enzyme (PFL-AE) with a peptide analog of PFL, which PFL-AE catalyzes H-atom abstraction to generate a peptide glycyl radical, as well as with a dehydroalanine-containing peptide substrate that promoted an alternative adenosylation reaction.[10,11]

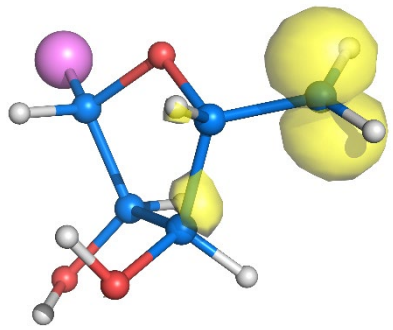

Figure 1. ***DFT model*** **of 5′-dAdo•**: ***Upper:*** Perspective view of optimized structure adapted from;[5] adenine represented by violet sphere, isosurface plot of the calculated HOMO (yellow) using an isodensity of 0.08 au.

Surprisingly, the highly reactive 5′-dAdo• formed by reductive cleavage of SAM during catalysis does not promptly react with substrate, **Scheme 1**. Instead, experiments on enzymes

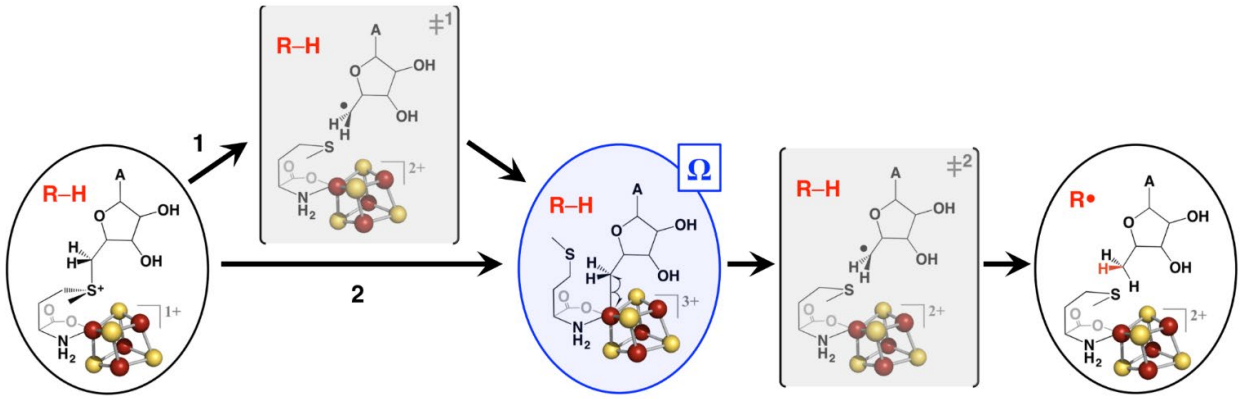

Scheme 1

broadly selected across the superfamily showed that substrate induced reductive cleavage of SAM generates, as the first trappable intermediate, the organometallic species Ω, in which the adenosyl 5′C is covalently bound to the unique iron of the [4Fe-4S] cluster; this may occur in a concerted fashion or via a 5′-dAdo• intermediate.[12,13,14] We have recently shown that it is the subsequent homolysis of the Fe-C5′ bond of Ω that releases 'free' 5′-dAdo• as the catalytically competent intermediate that directly reacts with substrate, with the radical having been observed both to insert into an olefinic peptide substrate and to abstract a glycyl H-atom from a peptide analog of PFL (RVSG$_{734}$YAV), which mimics glycyl radical formation on the native substrate, PFL.[10,11]

The ^{1}H and ^{13}C hyperfine parameters determined for 5′-dAdo• are completely characteristic of a radical with the odd electron localized in the 2pπ orbital of the C5′ sp^2 carbon, and those parameters are well matched by modern DFT computations for the isolated 5′-dAdo• radical.[5,15] Indeed, the initial report of the trapping and characterization of 5′-dAdo• concluded: "Perhaps the most surprising finding about 5′-dAdo• itself is the absence of surprises: its remarkable reactivity accompanies properties that are almost precisely as foundational studies of organic radicals long ago would have predicted." [16,17]

But, as we had shown, the 5′-dAdo• free radical in RS enzymes is never truly 'free': ENDOR measurements showed that tight van der Waals contact with its partners and active-site residues guide it in carrying out the exquisitely precise, regioselective reactions that are hallmarks of RS enzymes,[18] and similar guidance is operative in B$_{12}$ enzymes, as well.[19-22] Such active-site control in RS enzymes was first revealed by the observation that in the enzyme lysine 2,3-aminomutase (LAM) the spin on the stable but catalytically competent 5′-dAdo• surrogate, the allylic anhydroadenosyl radical (anAdo•), exhibits isotropic hyperfine couplings with ^{13}C, ^{2}H, and ^{15}N-labels of the lysine substrate, couplings that arise from electron-spin induced by anAdo• across the noncovalent contact interface with the atoms of Lys.[18] Such readily observed consequences of the tiny spin transfer from a paramagnetic center to a closed-shell neighbor not linked by a covalent bond were first revealed long ago, when it was found that $S = ½$ H atoms incorporated in a noble gas (e.g., Kr) matrix induce strong hyperfine coupling to matrix nuclei in the absence of covalent bond formation.[23,24] In the case of anAdo•, the van der Waals contact with the lysine substrate of LAM produced spin delocalization onto its 2-^{13}C that gave readily observable ^{13}C hyperfine couplings, yet is nonetheless so extremely small (2s spin density on 2-^{13}C, $\rho_{2s} \sim 10^{-3}$) as to leave the couplings to atoms of anAdo• unaltered.[25]

In the present report we extend such observations of the chaperoning of 5′-dAdo• by noncovalent contacts within its active-site environment through the detection and analysis of electron-spin induced by 5′-dAdo• onto neighboring products of SAM cleavage, through non-covalent interfaces within the pyruvate formate-lyase activating enzyme, **Scheme 2**, both in the absence of substrate and in the presence of the peptide substrate mimic, RVSG$_{734}$YAV. The *apparently* unexceptional 5′-dAdo• C5′ sp^2 carbon radical nonetheless is shown to strongly induce spin density on the $S = 0$ [4Fe-4S]$^{2+}$ cluster as revealed by the

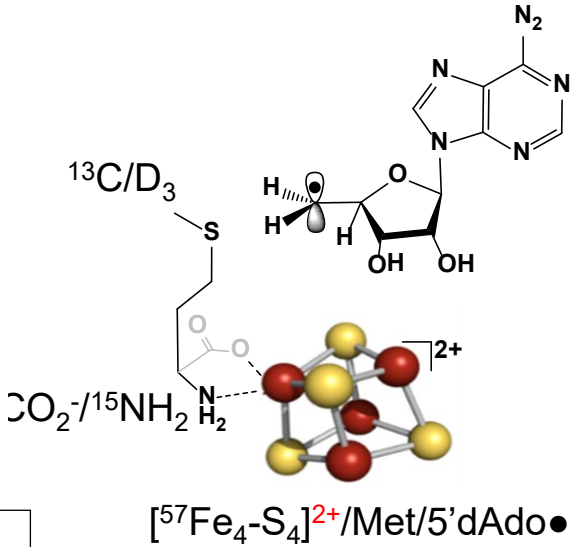

Scheme 2

influence of this spin density on the 5′-dAdo• g-tensor and as directly observed as ^{57}Fe hyperfine broadening of X-band EPR spectra and in Q-band ^{57}Fe ESEEM/ENDOR signals. In addition, proximity to the methionine cleavage product chelated to the $[4Fe\text{-}4S]^{2+}$ cluster is revealed by Q-band ENDOR signals from the methyl-group ^{13}C and $^{1/2}H_3$, the carboxyl ^{13}C, and the amino ^{15}N. The mechanism by which 5′-dAdo• induces spin density on the adjacent cluster is illuminated by a spin-coupling model that incorporates a weak exchange interaction between radical and cluster, as accompanied by BS-DFT computations.

The ENDOR-determination of through-space (dipolar) hyperfine couplings between the spin on 5′C of 5′-dAdo• and nuclei of the methionine cleavage product further allows us to create a structural model for the active-site positioning of the 5′-dAdo• after cleavage in the absence of substrate, with implications for the process leading to the formation of the organometallic intermediate, Ω that are supported by observation of enhanced interaction with the cluster in the presence of substrate. The results reveal that even in the absence of a substrate, 5′-dAdo• undergoes motion *towards* the unique Fe (Fe1) of the $[4Fe\text{-}4S]^{2+}$ cluster after S-C(5′) bond cleavage, with a resulting short C5′-to-Fe1 distance underlying the induction of spin onto the $S = 0$ cluster, while the presence of a peptide substrate modulates the position of the 5′-dAdo• so as to enhance the induced spin. This motion of the radical plausibly is an initial step in the formation of the Fe-C5′ bond of the organometallic intermediate, Ω.

Materials & Methods

Materials

All reagents were purchased from MilliporeSigma at the highest available purity unless otherwise noted. Methyl-D_3-L-methionine, methyl-^{13}C-L-methionine, carboxy-^{13}C-L-methionine, and ^{15}N-L-methionine were purchased from Isotec, and were used to synthesize the corresponding isotopically labeled SAMs as previously described.[26-28] Sodium dithionite was obtained from Acros Organics. Tris (hydroxymethyl) aminomethane (Tris) was purchased from Research Products International. All spectroscopy samples were prepared under an anaerobic atmosphere in a mBraun glove box (O_2 < 8 ppm) or in a COY chamber (O_2 < 10 ppm).

Expression and Purification of PFL-AE

Expression and purification of natural-abundance PFL-AE was carried out following a published protocol without modification.[26] ^{57}Fe-enriched PFL-AE was grown and purified using methods based on those previous described.[12,29] The pCAL-n-EK plasmid containing the PFL-AE gene was transformed into *E. coli* BL21(DE3)pLysS (Stratagene) cells for overexpression. A 50 mL LB and 50 μg/mL ampicillin starter culture grown overnight was used to inoculate 10 L of minimal media in a bench-top fermentor (New Brunswick) containing 50 μg/mL ampicillin and a solution of glucose and vitamins. The minimal media was previously described,[12] and contained 20 μM ^{57}Fe in place of natural abundance iron. The growth was incubated at 37°C with 250 rpm agitation and a flow of 5 L/min of compressed air to an OD_{600} of ~0.5, at which time isopropyl-β-D-thiogalactopyranoside (IPTG) was added to a final concentration of 0.5 mM and 20 μM ^{57}Fe (final concentration) was added. After ~2 hours, the cells were cooled and put under anaerobic conditions by purging the cells with N_2 once the culture reached ~ 30°C. Another addition of 20 μM ^{57}Fe (final concentration) was added once the culture reached ~20°C. The culture was purged with N_2 overnight at 4°C. The cells were harvested and stored in a -80°C freezer until purification. The ^{57}Fe-PFL-AE was purified from cell pellets as previously described.[12]

EPR Sample Preparation

At room temperature, a solution of PFL-AE was reduced with sodium dithionite for 8 mins before it was added to a solution of SAM in an X-band or Q-band EPR tube (Wilmad LabGlass). The resulting mixture of these solutions yielded a sample with the following concentrations: 225 μM PFL-AE, 6.75 mM sodium dithionite, 2.25 mM SAM in buffer (50 mM Tris-Cl, pH 8.5, 100 mM KCl, 10% glycerol). The samples were flash frozen in liquid nitrogen after mixing. Intra-cavity photolysis was carried out as previously.[5-7]

EPR/ENDOR Measurements

X-band CW EPR spectroscopy was conducted on a Bruker ESP 300 spectrometer equipped with an Oxford Instruments ESR 910, while Q-band CW EPR spectroscopy was conducted on a Bruker EMX spectrometer equipped with an Oxford Instruments Mercury iTC continuous helium flow cryostat. Typical experimental parameters were, T = 40 K, 9.38 GHz or 34.0 GHz, and 10 G modulation amplitude. EPR simulations were performed with the EasySpin[5.2.23] program operating in Matlab.[30]

35 GHz ESEEM and pulse ENDOR spectroscopic data were collected on spectrometers, described previously,[31-33] that are equipped with liquid helium immersion dewars for measurements at 2 K. For 35 GHz ESEEM spectra, a three-pulse sequence, $\pi/2 - \tau - \pi/2 - T - \pi/2$

- τ – echo, was employed with four-step phase cycling to suppress unwanted Hahn and refocused echoes. For a nucleus with nuclear spin of I = $^1/_2$ (^{57}Fe, ^{15}N,^{13}C), the ENDOR transitions for the $m_s = \pm^1/_2$ electron-spin manifolds are observed, to first order, at frequencies,

$$\upsilon_{\pm} = \left| \upsilon_{\mathrm{n}} \pm \frac{A}{2} \pm \left(\frac{3P(2\mathrm{M_I}) - 1}{2} \right) \right| \qquad (1a)$$

where ν_n is the nuclear Larmor frequency, and A is the hyperfine coupling. For I ≥ 1 (^{2}H, I = 1), the two ENDOR lines are further split by the nuclear quadrupole coupling (P) into 2I lines given by equation:

$$I \geq 1: \quad \upsilon_{\pm} = \left| \upsilon_{\mathrm{n}} \pm \frac{A}{2} \pm \left(\frac{3P(2\mathrm{M_I}) - 1}{2} \right) \right| \qquad (1b)$$

Calculations:

Broken symmetry – density functional theory (BS-DFT) calculations[34-36] were performed in vacuo using ORCA version 5.0.3.[37,38] Coordinates from a previously computed model complex were utilized, where geometry was optimized in the high-spin configuration as described.[39] In the current broken-symmetry calculations, the 5′dAdo group was truncated to a methyl radical and the distance of the methyl from the unique iron was set to that derived by ENDOR, as described; coordinates are given in **SI**. Broken-symmetry calculations were performed using the flipspin and finalms keywords.[37,38] Broken-symmetry calculations utilized the half-and-half Beck hybrid functional (BHandHLYP). [40] Atoms of the methyl radical were treated with the EPR-III basis set, while other C and H atoms were treated with the EPR-II basis set.[41] Fe and S atoms respectively were treated with the core properties basis set (CP(PPP)) and Ahlrichs' valence triple ξ with a polarization function (def2-TZVP) basis set.[42,43]

Results

Spin Density Induced by 5′-dAdo• on S = 0 [4Fe-4S]$^{2+}$co-Product of Reductive SAM Cleavage:

As we reported,[5] the X-band EPR spectrum of photogenerated natural-abundance 5′-dAdo• cryotrapped in the active site of PFL-AE is well reproduced with hyperfine coupling parameters, derived through isotopic substitution, fully characteristic of a 2pπ spin on the sp^2 5′C carbon of 5′-dAdo•, **Fig 2A, Table S1**, and we now find that the same is true for 5′-dAdo• trapped during the catalytic reaction with a bound PFL-analogue peptide, **Fig S1**, although intriguingly, with slightly altered hyperfine couplings (to be discussed). However, we did not note that the g-tensor required for the simulation of **Fig 2A** uncharacteristically had its unique value $g_{\|} > g_e$, whereas an isolated carbon-based radical, invariably has $g_{\|} < g_e$.[44,45] This omission was appropriate, given that the spread in field associated with this g-tensor at X-band is much smaller than the hyperfine couplings on which we focused, and thus the g-values were not highly precise. Indeed, collapsing the hyperfine couplings by perdeuterating the 5′-dAdo• does not yield an X-band spectrum that allows a better analysis of the g-tensor, **Fig 2A.**

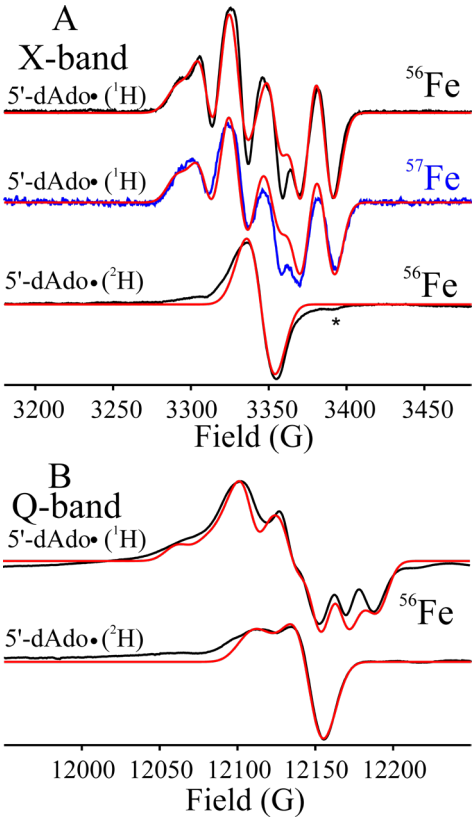

Figure 2. X-band EPR spectra of photogenerated natural-abundance 5′-dAdo• in the PFL-AE active site, with simulations (red): **A.** *(top)* Natural-abundance 5′-dAdo• , denoted (^{1}H), and [^{56}Fe$_4$S$_4$]$^{2+}$/Met; *(middle)* [^{57}Fe$_4$S$_4$]$^{2+}$/Met (middle, blue); *(bottom)* perdeuterated 5′-dAdo•, denoted (^{2}H), adjacent to [^{56}Fe$_4$S$_4$]$^{2+}$/Met. To ensure that the ^{57}Fe broadening is associated with 5′-dAdo• and is not compromised by the responses from un-photolyzed [4Fe-4S]$^{1+}$ cluster and other photogenerated species, any such contribution has been subtracted out, as follows. From the EPR spectra after photolysis has been subtracted the EPR spectra after annealing at 150K; at this temperature, 5′-dAdo• has decayed, while other species that contribute to a background remain (**Fig. S2**). **B**. Q-band EPR spectra of natural abundant 5′-dAdo• (top) and perdeuterated 5′-dAdo• (bottom) in the presence of [^{56}Fe$_4$S$_4$]$^{2+}$/Met. *Simulations* (red) for both X-band and Q-band EPR spectra achieved with **g** = [2.0075, 2.0015, 2.000] and hyperfine couplings compiled in **Table S1** (see text). X-band conditions: microwave frequency, 9.371 GHz, modulation, 10 G. Q-band conditions: microwave frequency, 34.01 GHz, modulation, 10 G. T = 40 K.

As shown in **Fig 2B, upper**, a loss of resolution in the Q-band spectrum of natural-abundance 5′-dAdo• defeats the use of the higher microwave frequency to refine the g-tensor of this species in natural isotopic abundance. However, the Q-band spectrum of perdeuterated 5′-dAdo• **(Fig 2B, lower)** allows such refinement, yielding an axial g-tensor with $g_{\|} = 2.0075 > g_{\perp} = 2.000$, that is strikingly different from those of hydrocarbon radicals, which are characterized by smaller g-shifts, as well as the 'reverse' symmetry, $g_{\|} < g_{\perp} \sim g_e$.[44,45] This suggested to us that the

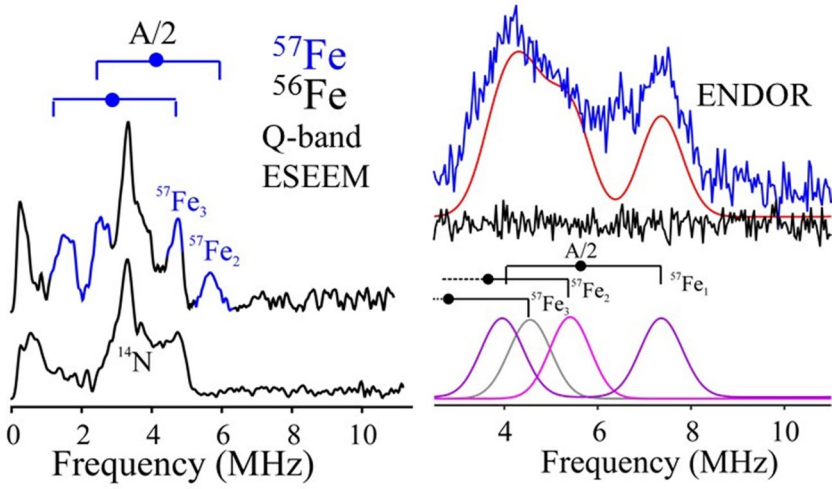

Figure 3. **Left panel,** ***(Upper)*** Q-band Fourier Transformed ESEEM spectra of photogenerated $[^{57}Fe_4S_4]^{2+}$/Met/5′-dAdo• in PFL-AE; features associated with two ^{57}Fe ions, denoted $^{57}Fe_3$ and $^{57}Fe_2$ are indicated with ^{57}Fe peaks marked as blue. ***(Lower)*** $[^{56}Fe_4S_4]^{2+}$/Met/5′-dAdo•. **Right Panel,** ***(Upper)*** Q-band Davies ENDOR spectra of $[^{57}Fe_4S_4]^{2+}$/Met/5′-dAdo• (Blue) and $[^{56}Fe_4S_4]^{2+}$/Met/5′-dAdo• (Black). Simulation (red): sum of ENDOR signals from three ^{57}Fe sites, two of which correspond to the sites observed in ESEEM. **(*Lower*),** Individual simulations of three individual ^{57}Fe signals, assuming: $a(^{57}Fe_3) = 5$ MHz, $a(^{57}Fe_2) = 7$ MHz, both couplings obtained from the ESEEM trace, and $a(^{57}Fe_1) = 12$ MHz; simulation was not attained by fitting the couplings to the ESEEM-observed sites. The 'goalposts' in both ESEEM and ENDOR spectra identify peaks of $\nu_\pm$ doublets (**eq 1b**) for individual ^{57}Fe ions, with doublet splitting $2\nu(^{57}Fe)$. Q-band 3-pulse ESEEM condition: microwave frequency, 34.51 GHz; pulse sequence, τ = 600 ns, T = 120 ns, incremented in 20 ns steps; Q-band ^{57}Fe Davies ENDOR condition: microwave frequency, 34.51 GHz; t_{180} =200 ns; τ = 800 ns, rep time, 20 ms. Both measurements, 2K.

g-tensor values might reflect contributions from interactions of 5′-dAdo• with the adjacent *S= 0* $[4Fe\text{-}4S]^{2+}$ cluster formed as the other product of photoinitiated reductive SAM cleavage. Frey and coworkers drew the corresponding inference that anAdo• trapped in the LAM active site experiences interactions with the $[4Fe\text{-}4S]^{2+}$ cluster based on the temperature-dependence of enhanced anAdo• electron-spin relaxation,[25] a phenomenon we likewise see for 5′-dAdo• in the present case (**Fig S3**).

To directly test for interactions between 5′-dAdo• and the *S= 0* $[4Fe\text{-}4S]^{2+}$ cluster, we collected X-band spectra from 5′-dAdo• prepared in enzyme that contained the isotopically enriched, $[^{57}Fe_4S_4]$ cluster, both in the absence of substrate and with bound substrate peptide. In the absence of this substrate the spectrum (**Fig 2A and Fig S1**) shows ^{57}Fe hyperfine broadening, definitively confirming that interaction of 5′-dAdo• with the S = 0 $[^{57}Fe_4S_4]^{2+}$ cluster generates unpaired spin on the $[^{57}Fe_4S_4]^{2+}$ cluster, while the EPR spectrum of 5′-dAdo• formed during enzymatic reaction with bound peptide PFL substrate-analog exhibits ^{57}Fe hyperfine broadening that is enhanced by the presence of the peptide (**Fig S1**). In the remainder of this Results section we focus on measurements carried out in the absence of substrate analogue, where 5′-dAdo• is stable as long as the sample remains frozen at 77 K and thus is amenable to extended study. In the

presence of peptide the 5′-dAdo• is highly reactive in the solid even at 77 K, forming the Gly• radical product on the peptide,[10,] and is not amenable to such studies. However, we return below to a comparison of the ^{57}Fe EPR linebroadening for the two enzyme states.

To determine the hyperfine couplings to cluster ^{57}Fe implied by the EPR linebroadening we employed Q-band ESEEM and ENDOR spectroscopies. The ESEEM frequency-domain spectrum of the isotopically enriched sample (**Fig 3, left**) clearly shows the presence of features from multiple ^{57}Fe, which overlay the ^{14}N background signals; **Fig S5** shows ESEEM data for several other values of τ. These ^{57}Fe ESEEM features can be assigned to two types of ^{57}Fe sites, with couplings, $a(^{57}Fe_3) = 5$ MHz, $a(^{57}Fe_2) = 7$ MHz; as the ^{57}Fe hyperfine couplings in FeS clusters are nearly isotropic,[35] the observed couplings can be treated as good approximations of the isotropic couplings. The ^{57}Fe Davies pulsed ENDOR response (**Fig 3, right**) can be simulated by inclusion of ν_+ peaks associated with Fe(2) and Fe(3) detected in the ESEEM data, plus an additional doublet with larger coupling, $a(^{57}Fe_1) \sim 12$ MHz. As a 'self-consistency' check, **Fig S1** shows that the ^{57}Fe broadening of the EPR spectrum (**Fig 2A**) is quite satisfactorily reproduced by incorporating these three ^{57}Fe hyperfine interactions; any coupling from the fourth Fe is presumably too small to influence the linewidth or to be clearly revealed in the ESEEM.

The origin of spin density on the [4Fe-4S]$^{2+}$ cluster:

As noted above, the ^{1}H and ^{13}C hyperfine parameters of 5-dAdo• are completely as expected for a radical with the odd electron localized in the 2pπ orbital of an sp^2 carbon,[5,15] and are well matched by DFT computations for the isolated radical.[5] Nonetheless, the measurements presented above show that the 5′-dAdo• radical induces unpaired spin density on the nominally *S = 0* [4Fe-4S]$^{2+}$ cluster: *(i)* the 5′-dAdo• EPR signal shows distinct ^{57}Fe hyperfine broadening upon ^{57}Fe enrichment of the active-site *S= 0* [4Fe-4S]$^{2+}$ cluster; *(ii)* ESEEM/ENDOR measurements show the ^{57}Fe broadening results from hyperfine-coupling to multiple ^{57}Fe of the cluster, not just the site-selected Fe that chelates SAM, with the largest coupling over a third the values expected for a paramagnetic [4Fe-4S]$^{1+/3+}$ cluster, and thus far too large to be the result of through-space dipolar interactions; [47 48] *(iii)* the 5′-dAdo• g-tensor has significant anisotropy, with $g'_{\|} = 2.0075 > g'_{\perp} = 2.000 \approx g_e$, whereas the deviations from g_e for an isolated carbon 2pπ-based radical are smaller and of the opposite sense, namely with $g_{\perp} > g_{\|} \approx g_e$.[44,45]

Given the completely unexceptional ^{1}H and ^{13}C hyperfine-coupling parameters for nuclei of the 5′-dAdo• radical, the observations that imply substantial spin density on the $[4Fe\text{-}4S]^{2+}$ cluster *cannot* result from significant direct delocalization of the nominally C5′-based radical spin onto the cluster, which would decrease those radical couplings. Instead, as we now explain, the *apparently* anomalous properties observed for 5′-dAdo• are the consequence of weak overlap between the radical wavefunction and that of the unique cluster Fe, which leads to a partial de-coupling of the local spins of the $S = 0$ $[4Fe\text{-}4S]^{2+}$ cluster and polarizes the local spins on the cluster ^{57}Fe ions, inducing hyperfine couplings to those ions.

The mechanism of this polarization is illustrated and illuminated by consideration of the simplified spin-coupling model shown in **Fig 4:** an $S_3 = ½$ radical in contact with a dinuclear cluster composed of two metal ions of identical spin, $S_1 = S_2 \equiv S_M$ whose interaction can be described by a strong, antiferromagnetic (AF) exchange coupling Hamiltonian,

$$\boldsymbol{H_0} = J\boldsymbol{S_1}\cdot\boldsymbol{S_2}\ (J > 0) \qquad (2a)$$

This intra-complex interaction gives an S = 0 cluster ground state and a manifold of excited states, $1 \leq S \leq 2S_M$, spaced in energy by multiples of J, whose magnitude is scaled by the repulsion between the unpaired electrons of the two cluster metal ions, **Fig 4**.

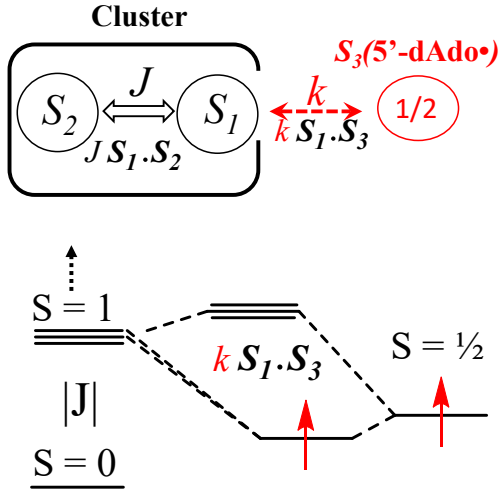

Figure 4: ***(upper)*** AF-coupled (J) di-nuclear cluster, ground-state $S = 0$, that experiences $S_1 \leftrightarrow S_3$(5′-dAdo•) exchange-coupling ($k\boldsymbol{S_1}\cdot\boldsymbol{S_2}$), ***(lower)*** Energy-level diagram showing interaction of radical spin with S = 1 cluster excited state.

We take one of the cluster ions, denoted M_1 ($\boldsymbol{S_1}$) as site-differentiated such that it is exposed to interaction with the nearby radical, just as is the case of 5′-dAdo• adjacent to the enzymatic $S = 0$ $[4Fe\text{-}4S]^{2+}$ cluster. This interaction can be described as a weak exchange coupling ($\boldsymbol{H_{mix}}$) between the local spin of M_1 ($\boldsymbol{S_1}$) and the 5′-dAdo• radical spin ($\boldsymbol{S_3}$), **eq 2b** and **Fig 4**, where $|k| < J$ is scaled by the overlap between the orbitals of the unpaired electrons on M_1 and that of the adjacent 5'-dAdo•,

$$\boldsymbol{H_{mix}} = k\,\boldsymbol{S_1}\cdot\boldsymbol{S_3} \qquad (2b)$$

This simple model is introduced to illustrate the key observation, that an *apparently* unperturbed radical in contact with the unique Fe-ion of an $S = 0$ cluster can nonetheless induce hyperfine couplings to both the Fe-ion in contact and the others as well. By extension such an interaction would induce couplings to all the Fe of an $S = 0$ $[4Fe\text{-}4S]^{2+}$ cluster, but the implementation of an $S = 0$ $[4Fe\text{-}4S]^{2+}$ cluster in the model would add complexity without adding insight. As noted, to achieve the model di-iron $S = 0$ ground state that corresponds to the $S = 0$ enzyme cluster, the two ions of the model must have identical spin. We treat both the mathematically simplest case, $S_M = ½$, which would correspond to a low-spin di-ferric cluster, and the slightly more complicated case of $S_M = 2$, corresponding to a cluster with two high-spin Fe^{2+} ions. By treating the latter case we show: *(i)* that the treatment can directly address a radical interacting with a high-spin Fe^{2+} ion, in what quite plausibly corresponds to interaction of 5′-dAdo•

with the unique Fe ion of the enzyme cluster;[39] *(ii)* that the induced cluster hyperfine couplings are enhanced by the higher-spin cluster Fe site; and *(iii)* that this spin-coupling model correlates with a BS-DFT treatment of a radical interacting with a diiron complex (the most complex system amenable to BS-DFT computation), as presented below.

In a first-order perturbation-theory treatment,[49,50] the coupling Hamiltonian **eq 2b** mixes the excited S = 1 state of the cluster into the wavefunction of the radical spin, **Fig 4** and **SI.** This mixing polarizes the local spins of *both* M ions of the *S= 0* cluster, which in turn induces hyperfine couplings of comparable magnitude but opposite sign to the two ions, **eq 3**, despite the fact that the radical interacts directly only with M_1 (**eq 2b**). If we consider the simplest case of two cluster metal ions with $S_M = ½$, for concreteness identifying them as low-spin Fe(III) ions, the expectation value of the ^{57}Fe hyperfine Hamilton gives as the observed ^{57}Fe couplings, $^{57}a_i$ (see **SI**)

$$ {}^{57}a_1 = -\frac{1}{2}\left(\frac{k}{|J|}\right){}^{57}\alpha_1 \quad ; \quad {}^{57}a_2 = +\frac{1}{2}\left(\frac{k}{|J|}\right){}^{57}\alpha_2 \qquad (3) $$

where the $^{57}a_i$ are the hyperfine couplings for the individual ^{57}Fe ions in the S = 1 cluster excited state. As these would be similar, then the two observed $^{57}a_i$ would be of comparable magnitude, but opposite in sign, even though the radical directly interacts only with Fe_1 (**eq 2b**). As noted directly below, the magnitudes of the coefficients differ with the choice of the spin of the component Fe ions, while the important feature of this equation does not – namely that the induced couplings are proportional to the ratio of the Fe_1 exchange coupling to the radical and the intra-dimer exchange coupling: $k/|J|$. Moreover, as the radical-Fe exchange coupling does not involve delocalization of the 5′-dAdo• spin, to first order in $|k/J|$ it leaves the radical's ^{1}H and ^{13}C hyperfine couplings essentially unperturbed by its interaction with the cluster, as observed experimentally.

As just noted, the constant multipliers, ±1/2 in the **eq 3** expressions for the $^{57}a_i$, vary with the values of S_M, while the proportionality to $k/|J|$ does not. In particular, for the dimer with S_M = 2, as would be associated with high-spin Fe(II), the coefficients in **eq 3** are (±2 √ 2), rather than (±1/2). Thus, this more realistic form of the model predicts substantially greater ^{57}Fe(II) hyperfine couplings for a given value of the perturbation parameter, $k/|J|$, helping to explain why a presumably weak radical-cluster exchange coupling can nonetheless give the considerable ^{57}Fe couplings observed experimentally. For illustrative purposes, consider the model's observed ^{57}Fe hyperfine couplings for a radical exchange-coupled to an $S = 0$ cluster (**eq 2b**) formed by exchange-coupling of two ferrous ions, $S_M = 2$, (**eq 2a**), and assign the hyperfine interaction in the $S = 1$ excited state to be $^{57}a_i \sim$ -20 MHz (the average cluster value, a_{test}, of Noodleman and Case[34-36]). Using coefficients for $S_M = 2$ in **eq 3**, then a 'median' value for the four observed hyperfine couplings observed by ENDOR for 5′-dAdo•, $|^{57}a_i| \sim 8$ MHz, would imply a ratio of exchange constants, $|k/J| \sim 0.14$. As also discussed in **SI**, the spin polarization of the S = 0 cluster through the radical↔M_1 interaction not only induces hyperfine couplings to the cluster metal ions, but also introduces contributions to the observed g-tensor, which explains the apparently anomalous g-values for 5′-dAdo•, $g'_{\|} > g'_{\perp} \sim g_e$.

The observed radical-cluster interaction, as incorporated in this model, is further illuminated by BS-DFT electronic-structure computations[34-36] on a corresponding molecular model, **Fig 5A**: a Rieske-like diiron center with two antiferromagnetically-coupled, high-spin (S =2) Fe(II) ions and total cluster spin, $S = 0$, interacting with an adjacent 'free' •CH_3 radical (S=1/2).

This model, which builds on a simplified model for the enzymatic intermediate Ω that was used in developing BS-DFT protocols for treating Ω itself, **Fig 5B,**[39] allows for spin transfer as well as exchange-induced spin polarization, and thus complements the spin-coupling approach of **Fig 4**.

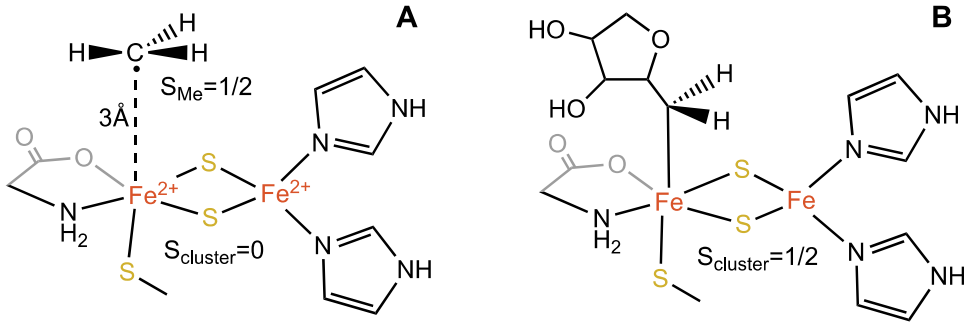

Figure 5. *Rieske*-based models for interaction of an alkyl moiety with a diiron center. **A)** Diferrous *Rieske*-based cluster model whose 'unique Fe' exhibits the same coordination sphere as the unique Fe of the [4Fe-4S] cluster after SAM cleavage, essentially in van der Waals contact with a methyl radical as stand-in for the spin-bearing C5′(H_2) of 5′-dAdo•. **B)** Rieske-based model of Ω, with C5′ of dAdo bonded to the 'unique' Fe of S = ½ mixed-valence dimer.

In these computations the carbon of the •CH_3 radical was placed 3 Å from the site-differentiated Fe of the *S= 0* $[4Fe\text{-}4S]^{2+}$ cluster, **Fig 5A**, a distance that corresponds to an ENDOR-derived result presented below for the distance between C5′ of 5′-dAdo• and the site-differentiated Fe of the *S= 0* PFL-AE $[4Fe\text{-}4S]^{2+}$ cluster. The hyperfine couplings for the methyl of the model were computed to be, $a_{iso}(^{13}C)$ = +97 MHz for the ^{13}C and $a_{iso}(^{1}H)$ = -68 MHz for the three equivalent methyl protons (**Table S3**), which reproduce quite well the values observed for a methyl radical trapped in the active site of HydG.[7] However, although the •CH_3 thus behaves as an 'ordinary radical', calculations nonetheless again show that, as with the exchange-coupling model of **Fig 4**, the radical-cluster interactions polarize the spins of the cluster without delocalizing the radical spin. This polarization induces isotropic ^{57}Fe hyperfine couplings to the two Fe ions that are of comparable magnitudes but opposite signs (**Table S3**), consistent with the ENDOR/ESEEM measurements, and with the predictions of the spin-coupling model above (**eq 3**).

Overall, the treatment of the spin-coupling model of **Fig 4**, in combination with the DFT computations on the molecular model of **Fig 5A**, thus explain the observation that the EPR spectrum of the ostensibly 'free' 5′-dAdo• radical nonetheless exhibits ^{57}Fe EPR broadening and hyperfine interactions with multiple ^{57}Fe ions of the adjacent S = 0, $[4Fe\text{-}4S]^{2+}$ cluster (**Fig 3**), as well as g-values shifted from those of an isolated carbon 2pπ free radical, yet does so without significantly diminishing the radical's ^{1}H and ^{13}C hyperfine couplings through spin-density delocalization onto the cluster. They further suggest that variation in the active site among enzymes likely would modulate the cluster-radical interaction strength, k, causing the ^{57}Fe broadening and g-shifts to vary among members of the superfamily.

5'-dAdo• Hyperfine Interactions With Methionine co-Product of Reductive SAM Cleavage:

The 5′-dAdo• radical was generated from SAMs isotopically labelled on the methionine methyl (^{13}C or ^{2}H) or the amino-acid terminus (^{13}C carboxyl or $^{15}NH_2$), through photoinduced electron transfer from the $[4Fe\text{-}4S]^{1+}$ cluster to the bound SAM. ENDOR spectra of the resulting

5′-dAdo• radicals revealed hyperfine couplings to the isotopic labels of the methionine co-product situated in van der Waals contact, **Scheme 2**. **Figure 6** presents the Q-band ^{15}N, ^{13}C, and ^{2}H ENDOR spectra from the labelled samples, along with simulations that employed the corresponding hyperfine tensors listed in **Table 1**. Simulation of the ^{13}C and ^{15}N spectra is particularly straightforward. At the distances of interest, the hyperfine coupling to each of these nuclei is describable as the interaction of a point electron spin on C5' with a single I = ½ nucleus. This interaction is described by a point-dipole axial tensor, with magnitude determined only by distance, with the possibility of an added isotropic term. As the g-anisotropy for 5′-dAdo• is less than the ^{1}H hyperfine-determined breadth of its EPR spectrum even at Q-band, the spectra are without orientation selection, and those of ^{13}C and ^{15}N thus have well-defined patterns –versions of the classic 'Pake-pattern'[49] – whose simulations accurately yield the full (axial) distance-dependent hyperfine tensors (**eqs 5, 6**, below). In short, the nature of the present problem of determining ^{13}C and ^{15}N distances from C5′ eliminates all the typical issues of more complex ENDOR measurements – enabling the excellent fits of **Fig 6** and resulting in well-defined estimates of those C5′-nuclear distances.

Table 1. Hyperfine coupling parameters for the ENDOR simulations of **Fig 6.**

Nucleus	A1,A2,A3 (MHz)	a_{iso} (MHz)	2T,-T,-T (MHz)
$^{13}CH_3$	0.6,-1.4,-1.4	-0.73	1.33, -0.67,-0.67
$CD_3(^2H_a)$	1.34,-0.52,-0.52 [a]	0.1	1.24,-0.62,-0.62,
$CD_3(^2H_b)$	1.02,-0.36,-0.36 [a]	0.1	0.92,-0.46, -0.46
$CD_3(^2H_c)$	0.48,-0.09,-0.09 [a]	0.1	0.38,-0.19,-0.19
Carboxyl ^{13}C	0.9,-1.22,-1.22	-0.51	1.41,-0.71,-0.71
Amino ^{15}N	0.2,-0.1,-0.1	~ 0	0.2,-0.1,-0.1

[a] ^{2}H tensors are not used in determination of the C-5′ positioning, **eqs 4, 5**.

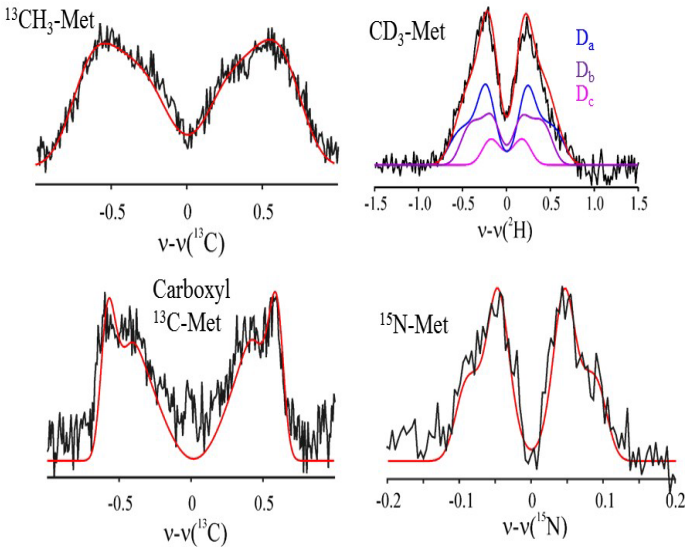

Figure 6. *(Top left)* Q-band ^{13}C Mims ENDOR spectra of $[4Fe\text{-}4S]^{2+}/^{13}CH_3$-Met/5′-dAdo•; *(Top right)* Q-band ^{2}H Mims ENDOR spectra of $[4Fe\text{-}4S]^{2+}/CD_3$-Met/5′-dAdo•; *(Bottom left)* Q-band ^{13}C Mims ENDOR spectra of $[4Fe\text{-}4S]^{2+}$/ carboxyl-^{13}C-Met/5′-dAdo•; *(Bottom right)* Q-band ^{15}N ENDOR spectra of $[4Fe\text{-}4S]^{2+}/^{15}N$-Met/5′-dAdo•. *ENDOR simulations* done with *EasySpin* using hyperfine tensors in **Table 1**. For the ^{2}H ENDOR simulation of $[4Fe\text{-}4S]^{2+}/$ CD_3-Met/5′-dAdo•, a_{iso} is maintained the same for D_a (blue), D_b (purple), and D_c (pink) of CD_3; their simulation sum is rendered as red. *Q-band Mims ENDOR condition:* microwave frequency, 34.55 GHz; t_{90} = 50 ns; rep time, 30 ms; τ = 450 ns (^{13}C), 500 ns (^{2}H) and 800 ns (^{15}N). T = 2K.

The simulations indicate the presence of isotropic couplings to the ^{13}C (and $^{1/2}H$ nuclei) of the methionine methyl group (**Table 1**), revealing that this group, too, is in tight van der Waals contact with the C5′ 2pπ atomic orbital of 5′-dAdo•. The couplings are attributable to 'Pauli spin delocalization' that is introduced by orthogonalization of the radical and methionine-methyl orbitals, and which delocalizes the spin.[23,24,51] However, the magnitude of the spin delocalization giving rise to the isotropic couplings of the methionine nuclei (~10^{-3} of a spin) is far too small to alter the couplings to nuclei of 5′-dAdo•.

The magnitude of spin residing on the methionine nuclei is far too small to account for the anisotropic hyperfine couplings to the methyl nuclei (**Table 1**). Instead those couplings must be assigned to the through-space dipolar interaction with the C5′ spin, which is described by the tensor of axial form,[52]

$$\boldsymbol{T} = [-T, -T, 2T] \qquad (4)$$

The parameter T is related to the distance *r* from C5′ to the nucleus being examined through the relationship,

$$T(r) = g_e g_N \beta_e \beta_N \frac{\rho(C5')f(r)}{r^3} \qquad (5)$$

where ρ(C5′) = 0.7 is the spin density on C5′ of 5′-dAdo•.[5] The factor, *f(r)* <1 takes into account the distributed nature of the spin in the 2pπ orbital of C5′,[16,17] and has the effect of decreasing a calculated distance, *r*, by ~ 0.1 Å relative to that calculated from a measured value of T without its incorporation. **Table 2** lists the distances from C5′ to the methionine nuclei interrogated by ENDOR both in the crystal structure of the parent enzyme with its [4Fe-4S]$^{1+}$/SAM complex, and as determined by ENDOR of the 5′-dAdo• radical in the state formed by photoinduced SAM cleavage.

Table 2 Distances from C5′ of SAM to the nuclei of methionine and calculated distance to the unique Fe

Nucleus (X)	[a]C5′↔X distance (Å) of SAM/$[Fe_4S_4]^{1+}$	[b]C5′↔X distance (Å) Post cleavage
Amino N	5.1	3.8
Carboxyl C	4.1	2.7
methyl C	2.8	2.7
unique Fe	5.1	2.9[c]

[a] The distance from crystallographic structure[49]
[b] The distance from ENDOR measurement (this work)
[c] As described in text, the distance is inferred from computationally modeling the [4Fe-4S]$^{2+}$/Met/5′-dAdo• center using the ENDOR measurement.

Summary, Metrical Insights, and Conclusions

^{1}H and ^{13}C hyperfine couplings for nuclei of the 5′-dAdo• radical enveloped in the active site of the RS enzyme PFL-AE are completely characteristic of a classical 'free' organic radical that has an unpaired electron localized in the 2pπ orbital of the C5′ sp^2 carbon, as illustrated by the large ^{13}C-5′ hyperfine coupling constant, $\boldsymbol{A}$ = [10,10,230] MHz.[5,15] Yet this 'unexceptional' radical nonetheless is here found to exhibit substantial ^{57}Fe, ^{13}C, ^{2}H, and ^{15}N hyperfine couplings to the adjacent, non-covalently bound, isotopically-labelled methionine-bound [4Fe-4S]$^{2+}$ complex generated by the homolytic cleavage of cluster-bound SAM that generates 5′-dAdo•. The generation of ^{57}Fe couplings across a tight van der Waals interface to the cluster, as illuminated through the exchange-coupling and molecular models above, deepens our understanding of the degree to which the active site of a radical SAM enzyme chaperones a 5′-dAdo• radical through van der Waal contacts with neighbors that are so intimate as to induce electron-spin on those neighbors. The importance of these interactions in catalysis is confirmed by the observation that 5′-dAdo• generated during enzymatic H-atom abstraction from a peptide analog of PFL[13] also exhibits close contacts with the [4Fe-4S]$^{2+}$, as evidenced by ^{57}Fe broadening (**Fig S2**).

To visualize the contacts involved, we employed the ENDOR-derived distances between C5′ of the photogenerated 5′-dAdo• radical and the hyperfine-coupled neighboring methionine atoms (**Table 2**) as structural constraints in determining the positioning of the C5′ radical relative to the [4Fe-4S]$^{2+}$ cluster, an analogous procedure to that used to position the product 5′-dAdo relative to a substrate radical in a B_{12} enzyme.[22] As a starting point, we assumed that the methionine

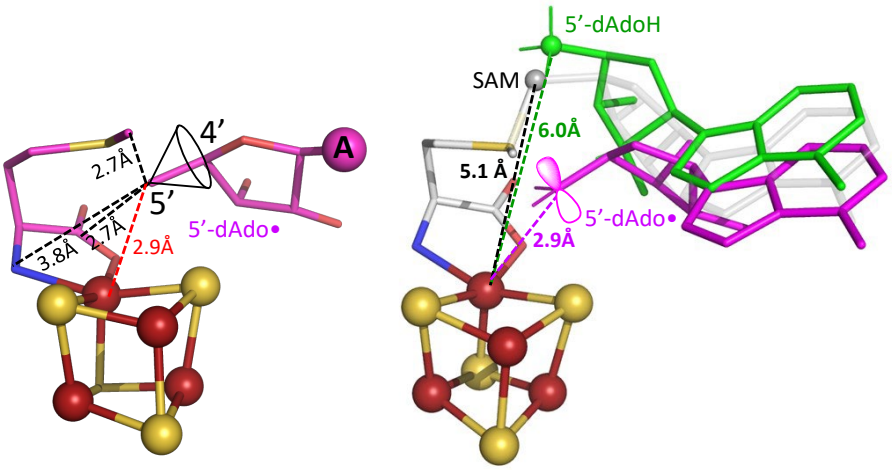

Fig 7: Left, Structural model of 5′-dAdo• position relative to the methionine-bound [4Fe-4S]$^{2+}$ as derived by imposing the ENDOR-derived distances from C5′ relative to the amino nitrogen (3.8 Å), carboxy carbon (2.7 Å) and methyl carbon (2.7 Å); The adenine moiety is represented by the purple ball (A). The distance from C5′ to the unique Fe thus determined is 2.9 Å. **Right,** overlap of the structure of SAM-bound [4Fe-4S]$^{2+}$ cluster (transparent gray, PDB 8FSI),[54] 5′-dAdoH (green, PDB 8FO0)[54] and the 5′-dAdo• model (purple). The initial Fe-C5′ distance of 5.1 Å in the SAM complex (gray) is shortened to Fe-C5′= 2.9 Å after SAM cleavage to generate 5′-dAdo• (purple), a step towards formation of Ω, while the Fe-C5′ distance has relaxed to 6.0 Å after completion of the hydrogen abstraction reaction to form 5′-dAdoH (green).

product of SAM photo-homolysis would undergo minimal movement in the 12 K frozen sample, and superimposed a DFT-optimized structure of 5′-dAdo• (**Fig 1**)[5] onto the methionine-bound [4Fe-4S] cluster of the crystallographically-determined parent structure with SAM bound to the

[4Fe-4S] cluster[53,54] using PyMOL.[55] It proved possible to position the 5′C of 5′-dAdo• relative to the methionine-bound [4Fe-4S] cluster with minimal motions of the adenine, by sliding 5′-dAdo• and twisting the ribose ring with respect to the adenine so as to simultaneously satisfy the *complete set* of ENDOR-derived distance constraints: the 5′C distances derived from the dipolar couplings between the unique cluster Fe and the methionine methyl ^{13}C, amino ^{15}N, and carboxy ^{13}C (**Table 2**). **Fig 7, Left**, illustrates the resulting model for the active-site positioning of 5′C of 5′-dAdo• after SAM cleavage, while **Fig 7, right** and **Fig S6** show the modeled structure of the 5′-dAdo• intermediate state overlaid with structures[54] of the SAM-bound cluster (prior to reductive cleavage, gray) and the methionine-bound cluster and 5′-dAdoH product of H-atom abstraction (after turnover, green) as presented from several perspectives.

The frozen matrix, with its tight contacts between radical and surroundings, allows C5' of the liberated radical to move ~2 Å towards the Fe from its initial position ~ 5 Å away, a substantial portion of the distance needed to form the Fe-C5' bond of Ω, yet prevents actual formation of that organometallic intermediate. The Ω intermediate, in contrast, is freeze-trapped during reaction with substrate at ambient temperatures where the constraints of the frozen matrix are not operative. The nonetheless shortened 5′-dAdo• (C5′)-Fe1 distance of ~2.9 Å seen here after photoreductive SAM cleavage introduces the quantum-mechanical coupling between radical and cluster that generates the surprising isotropic hyperfine coupling between the completely characteristic 5′-dAdo• sp^2 carbon electron-spin and the ^{57}Fe nuclear spins of the S = 0 [4Fe-4S]$^{2+}$ cluster; correspondingly, the short distance between C5′ and the methyl ^{13}C of the methionyl SAM cleavage product is consistent with its observed isotropic hyperfine coupling. However, it is perhaps useful to emphasize that the coupling to the [4Fe-4S]$^{2+}$ cluster induced at the ~2.9 Å Fe-C5′ distance determined by ENDOR by no means reflects a true Fe-C5′ covalent bond, such as exists in the organometallic complex Ω, a central intermediate in catalysis by radical-SAM enzymes. Among the multiple properties listed in **Table S2** that distinguish the 'free' 5′-dAdo• here trapped in proximity to the cluster, from the 5′-dAdo group of Ω, with C5′ coordinated to the unique cluster-Fe, the most obvious is their ^{13}C5′ hyperfine coupling constants: a_{iso}(^{13}C5′)= 83 MHz for the 'free' 5′-dAdo• and a_{iso}(^{13}C5′) = 9 MHz for Ω. This difference demonstrates that in the case of 'free' 5′-dAdo•, most of the electron spin is localized on the 5′-C, whereas in Ω, most of the spin is on the [4Fe-4S]$^{3+}$ cluster.

The structural model for the product of SAM photocleavage described here does, however, provide insight into the process by which Ω forms subsequent to SAM cleavage during catalysis. As shown in **Fig 7, right**, this model displays a substantial motion of the radical-bearing C5′ *towards* the unique Fe of the [4Fe-4S]$^{2+}$ cluster upon homolytic cleavage of SAM to form 5′-dAdo•, plausibly an initial step towards the formation of the Fe-C5′ bond of the Ω organometallic intermediate. This movement would be consistent with the generally accepted model for enzymatic reductive cleavage of SAM, which involves movement of the sulfonium towards the [4Fe-4S]$^{+}$ cluster to promote the electron transfer from the cluster to the sulfonium that causes reductive cleavage of the S-C5′ bond.[2,3,6,56-58] It is interesting, however, that a recent crystal structure of the PFL-AE post-reductive cleavage complex with 5′-dAdoH and the methionine-bound [4Fe-4S] cluster shows that C5′ of the 5′-dAdoH product relaxes to a position even farther from the cluster-Fe than the distance of C5′ of SAM prior to cleavage (**Fig 7 right**).[54]

Overall, the metrical information presented here are consistent with a model in which the initiating process of enzymatic SAM reductive cleavage moves the resulting 5′-dAdo• towards the [4Fe-4S] cluster, leading to formation of the organometallic intermediate Ω. Subsequent homolysis

of the Fe-C5′ bond of Ω then liberates the 5′-dAdo• intermediate, which moves away from the cluster to abstract an H• from substrate (**Scheme 1**).

Acknowledgements:
M.N.L. (F32GM140713) and M.B.H. (T32GM008382) were supported by the NIH. J.B.B. thanks the NIH (R35 GM131889) for support. B.M.H thanks the NIH (2 R01 GM111097), and also the NSF (MCB-1908587), for support.

ASSOCIATED CONTENT

Supporting Information: The Supporting Information is available free of charge at https://pubs.acs.org
Six figures, four tables, a discussion of the perturbation treatment of the exchange-coupled model, and a discussion of BS-DFT computations.

AUTHOR INFORMATION

Corresponding Authors:

Brian M. Hoffman – Department of Chemistry, Northwestern University, Evanston, Illinois 60208, United States; orcid.org/0000-0002-3100-0746; Email: bmh@ northwestern.edu

Joan B. Broderick: Department of Chemistry and Biochemistry, Montana State University, Bozeman, Montana 59717, United States; htttps://orcid.org/0000-0001-7057-9124; Email: jbroderick@montana.edu

Authors:

Hao Yang - Department of Chemistry, Northwestern University, Evanston, Illinois 60208, United States; https://orcid.org/0000-0001-7229-0957

Maike N. Lundahl – Department of Chemistry and Biochemistry, Montana State University, Bozeman, Montana 59717, United States; https://orcid.org/0000-0002-4391-7279

Madeline B. Ho – Department of Chemistry, Northwestern University, Evanston, Illinois 60208, United States; https://orcid.org/0000-0001-6351-2132

William E. Broderick: Department of Chemistry and Biochemistry, Montana State University, Bozeman, Montana 59717, United States; https://orcid.org/0000-0001-5782-7322

References

(1) Broderick, J. B.; Duffus, B. R.; Duschene, K. S.; Shepard, E. M. Radical S-Adenosylmethionine Enzymes. *Chem Rev* **2014**, *114*, 4229-4317. DOI: 10.1021/cr4004709.

(2) Broderick, J. B.; Broderick, W. E.; Hoffman, B. M. Radical SAM Enzymes: Nature's Choice for Radical Reactions. *FEBS Lett* **2022**, *597*, 92-101. DOI: 10.1002/1873-3468.14519.

(3) Hoffman, B. M.; Broderick, W. E.; Broderick, J. B. Mechanism of Radical Initiation in the Radical SAM Enzyme Superfamily. *Annu. Rev. Biochem.* **2023**, *92*, 333-349. DOI: 10.1146/annurev-biochem-052621-090638.

(4) Magnusson, O. T.; Reed, G. H.; Frey, P. A. Spectroscopic Evidence for the Participation of an Allylic Analogue of the 5'-Deoxyadenosyl Radical in the Reaction of Lysine 2,3-Aminomutase. *J. Am. Chem. Soc.* **1999**, *121*, 9764-9765. DOI: Doi 10.1021/Ja9925507.

(5) Yang, H.; McDaniel, E. C.; Impano, S.; Byer, A. S.; Jodts, R. J.; Yokoyama, K.; Broderick, W. E.; Broderick, J. B.; Hoffman, B. M. The Elusive 5'-Deoxyadenosyl Radical: Captured and Characterized by Electron Paramagnetic Resonance and Electron Nuclear Double Resonance Spectroscopies. *J. Am. Chem. Soc.* **2019**, *141*, 12139-12146. DOI: 10.1021/jacs.9b05926.

(6) Impano, S.; Yang, H.; Jodts, R. J.; Pagnier, A.; Swimley, R.; McDaniel, E. C.; Shepard, E. M.; Broderick, W. E.; Broderick, J. B.; Hoffman, B. M. Active-Site Controlled, Jahn-Teller Enabled Regioselectivity in Reductive S-C Bond Cleavage of S-Adenosylmethionine in Radical SAM Enzymes. *J. Am. Chem. Soc.* **2021**, *143*, 335-348. DOI: 10.1021/jacs.0c10925.

(7) Yang, H.; Impano, S.; Shepard, E. M.; James, C. D.; Broderick, W. E.; Broderick, J. B.; Hoffman, B. M. Photoinduced Electron Transfer in a Radical SAM Enzyme Generates an S-Adenosylmethionine Derived Methyl Radical. *J. Am. Chem. Soc.* **2019**, *141*, 16117-16124. DOI: 10.1021/jacs.9b08541.

(8) Impano, S.; Yang, H.; Shepard, E. M.; Swimley, R.; Pagnier, A.; Broderick, W. E.; Hoffman, B. M.; Broderick, J. B. S-Adenosyl-L-Ethionine Is a Catalytically Competent Analog of S-Adenosyl-L-Methione (SAM) in the Radical SAM Enzyme HydG. *Angew Chem Int Ed Engl* **2021**, *60*, 4666-4672. DOI: 10.1002/anie.202014337.

(9) Sayler, R. I.; Stich, T. A.; Joshi, S.; Cooper, N.; Shaw, J. T.; Begley, T. P.; Tantillo, D. J.; Britt, R. D. Trapping and Electron Paramagnetic Resonance Characterization of the 5'-dAdo• Radical in a Radical S-Adenosyl Methionine Enzyme Reaction with a Non-Native Substrate. *ACS Cent Sci* **2019**, *5*, 1777-1785. DOI: 10.1021/acscentsci.9b00706.

(10) Lundahl, M. N.; Yang, H.; Broderick, W. E.; Hoffman, B. M.; Broderick, J. B. Pyruvate Formate-Lyase Activating Enzyme: The Catalytically Active 5´-Deoxyadenosyl Radical Caught in the Act of H-Atom Abstraction. *PNAS* **2023,***120*, e2314696120; https://doi.org/10.1073/pnas.2314696120.

(11) Lundahl, M. N.; Sarksian, R.; Yang, H.; Jodts, R. J.; Pagnier, A.; Smith, D. F.; Mosquera, M. A.; van der Donk, W. A.; Hoffman, B. M.; Broderick, W. E.; Broderick, J. B. Mechanism of Radical S-Adenosyl-L-Methionine Adenosylation: Radical Intermediates and the Catalytic Competence of the 5'-Deoxyadenosyl Radical. *J. Am. Chem. Soc.* **2022**, *144*, 5087-5098. DOI: 10.1021/jacs.1c13706.

(12) Horitani, M.; Shisler, K.; Broderick, W. E.; Hutcheson, R. U.; Duschene, K. S.; Marts, A. R.; Hoffman, B. M.; Broderick, J. B. Radical SAM Catalysis Via an Organometallic Intermediate with an Fe-[5'-C]-Deoxyadenosyl Bond. *Science* **2016**, *352*, 822-825. DOI: 10.1126/science.aaf5327.

(13) Byer, A. S.; Yang, H.; McDaniel, E. C.; Kathiresan, V.; Impano, S.; Pagnier, A.; Watts, H.; Denler, C.; Vagstad, A. L.; Piel, J.; Duschene, K. S.; Shepard, E. M.; Shields, T. P.; Scott, L. G.; Lilla, E. A.; Yokoyama, K.; Broderick, W. E.; Hoffman, B. M.; Broderick, J. B. Paradigm Shift for Radical S-Adenosyl-L-Methionine Reactions: The Organometallic Intermediate Omega Is Central to Catalysis. *J. Am. Chem. Soc.* **2018**, *140*, 8634-8638. DOI: 10.1021/jacs.8b04061.

(14) Pagnier, A.; Yang, H.; Jodts, R. J.; James, C. D.; Shepard, E. M.; Impano, S.; Broderick, W. E.; Hoffman, B. M.; Broderick, J. B. Radical SAM Enzyme Spore Photoproduct Lyase: Properties of

the Omega Organometallic Intermediate and Identification of Stable Protein Radicals Formed During Substrate-Free Turnover. *J. Am. Chem. Soc.* **2020**, *142*, 18652-18660. DOI: 10.1021/jacs.0c08585.

(15) Cole, T.; Heller, C.; McConnell, H. M. Electron Magnetic Resonance of $CH(COOH)_2$. *PNAS* **1959**, *45*, 525-528.

(16) McConnell, H. M.; Heller, C.; Cole, T.; Fessenden, R. W. Radiation Damage in Organic Crystals .1. $CH(COOH)_2$ in Malonic Acid. *J. Am. Chem. Soc.* **1960**, *82*, 766-775. DOI: Doi 10.1021/Ja01489a002.

(17) McConnell, H. M.; Strathdee, J. Theory of Anisotropic Hyperfine Interactions in π-Electron Radicals. *Mol. Phys.* **1959**, *2*, 129-138. For Erratum, see R. M. Pitzer, C. W. Kern and W. N. Lipscomb, *J. Chem. Phys.* 1*37*, 267 (1962).

(18) Horitani, M.; Byer, A. S.; Shisler, K. A.; Chandra, T.; Broderick, J. B.; Hoffman, B. M. Why Nature Uses Radical SAM Enzymes So Widely: Electron Nuclear Double Resonance Studies of Lysine 2,3-Aminomutase Show the 5'-dAdo• "Free Radical" Is Never Free. *J. Am. Chem. Soc.* **2015**, *137*, 7111-7121. DOI: 10.1021/jacs.5b00498.

(19) Rétey, J. Enzymic Reaction Selectivity by Negative Catalysis or How Do Enzymes Deal with Highly Reactive Intermediates? *Angewandte Chemie International Edition in English* **1990**, *29*, 355-361. DOI: https://doi.org/10.1002/anie.199003551.

(20) Bucher, D.; Sandala, G. M.; Durbeej, B.; Radom, L.; Smith, D. M. The Elusive 5′-Deoxyadenosyl Radical in Coenzyme-B12-Mediated Reactions. *J. Am. Chem. Soc.* **2012**, *134*, 1591-1599. DOI: 10.1021/ja207809b.

(21) Buckel, W.; Friedrich, P.; Golding, B. T. Hydrogen Bonds Guide the Short-Lived 5'-Deoxyadenosyl Radical to the Place of Action. *Angew Chem Int Ed Engl* **2012**, *51*, 9974-9976. DOI: 10.1002/anie.201205299.

(22) Warncke, K.; Utada, A. S. Interaction of the Substrate Radical and the 5'-Deoxyadenosine-5'-Methyl Group in Vitamin B12 Coenzyme-Dependent Ethanolamine Deaminase. *J. Am. Chem. Soc.* **2001**, *123*, 8564-8572.

(23) Foner, S. N.; Cochran, E. L.; Bowers, V. A.; Jen, C. K. Multiple Trapping Sites for Hydrogen Atoms in Rare Gas Matrixes. *J. Chem. Phys.* **1960**, *32*, 963-971. DOI: 10.1063/1.1730905.

(24) Morton, J. R.; Preston, K. F.; Strach, S. J.; Adrian, F. J.; Jette, A. N. Anisotropic Hyperfine Interactions of Rare-Gas Nuclei near Trapped Hydrogen Atoms. *J. Chem. Phys.* **1979**, *70*, 2889-2893. DOI: 10.1063/1.437825.

(25) Magnusson, O. T.; Reed, G. H.; Frey, P. A. Characterization of an Allylic Analogue of the 5'-Deoxyadenosyl Radical: An Intermediate in the Reaction of Lysine 2,3-Aminomutase. *Biochemistry* **2001**, *40*, 7773-7782. DOI: 10.1021/bi0104569.

(26) Byer, A. S.; McDaniel, E. C.; Impano, S.; Broderick, W. E.; Broderick, J. B.: Chapter Ten - Mechanistic Studies of Radical SAM Enzymes: Pyruvate Formate-Lyase Activating Enzyme and Lysine 2,3-Aminomutase Case Studies. In *Methods Enzymol.*; Bandarian, V., Ed.; Academic Press, 2018; Vol. 606; pp 269-318.

(27) Walsby, C. J.; Ortillo, D.; Broderick, W. E.; Broderick, J. B.; Hoffman, B. M. An Anchoring Role for FeS Clusters: Chelation of the Amino Acid Moiety of S-Adenosylmethionine to the Unique Iron Site of the [4Fe-4S] Cluster of Pyruvate Formate-Lyase Activating Enzyme. *J. Am. Chem. Soc.* **2002**, *124*, 11270-11271.

(28) Walsby, C. J.; Hong, W.; Broderick, W. E.; Cheek, J.; Ortillo, D.; Broderick, J. B.; Hoffman, B. M. Electron-Nuclear Double Resonance Spectroscopic Evidence That S-Adenosylmethionine Binds in Contact with the Catalytically Active $[4Fe{-}4S]^{+}$ Cluster of Pyruvate Formate-Lyase Activating Enzyme. *J. Am. Chem. Soc.* **2002**, *124*, 3143-3151. DOI: 10.1021/ja012034s.

(29) Krebs, C.; Henshaw, T. F.; Cheek, J.; Huynh, B. H.; Broderick, J. B. Conversion of 3Fe-4S to 4Fe-4S Clusters in Native Pyruvate Formate-Lyase Activating Enzyme: Moessbauer Characterization and Implications for Mechanism. *J. Am. Chem. Soc.* **2000**, *122*, 12497-12506.

(30) Stoll, S.; Schweiger, A. Easyspin, a Comprehensive Software Package for Spectral Simulation and Analysis in EPR. *J. Magn. Reson.* **2006**, *178*, 42-55. DOI: 10.1016/j.jmr.2005.08.013.

(31) Werst, M.; Davoust, C. E.; Hoffman, B. M. Ligand Spin Densities in Blue Copper Proteins by Q-Band Proton and Nitrogen-14 ENDOR Spectroscopy. *J. Am. Chem. Soc.* **1991**, *113*, 1533-1538. DOI: 10.1021/ja00005a011.

(32) Zipse, H.; Artin, E.; Wnuk, S.; Lohman, G. J. S.; Martino, D.; Griffin, R. G.; Kacprzak, S.; Kaupp, M.; Hoffman, B.; Bennati, M.; Stubbe, J.; Lees, N. Structure of the Nucleotide Radical Formed During Reaction of Cdp/Ttp with the E441q-A2b2 of *E. Coli* Ribonucleotide Reductase. *J. Am. Chem. Soc.* **2009**, *131*, 200-211.

(33) Davoust, C. E.; Doan, P. E.; Hoffman, B. M. Q-Band Pulsed Electron Spin-Echo Spectrometer and Its Application to ENDOR and ESEEM. *Journal of Magnetic Resonance Series A* **1996**, *119*, 38-44. DOI: DOI 10.1006/jmra.1996.0049.

(34) Noodleman, L.; Case, D. A.: Local Density Functional Approaches to Spin Coupling in Transition Metal Clusters. In *Theory and Applications of Density Functional Approaches to Chemistry*; Labanowski, J. K., Andzelm, J. W., Eds.; Springer Verlag, 1991.

(35) Mouesca, J. M.; Noodleman, L.; Case, D. A.; Lamotte, B. Spin-Densities and Spin Coupling in Iron-Sulfur Clusters - a New Analysis of Hyperfine Coupling-Constants. *Inorg. Chem.* **1995**, *34*, 4347-4359. DOI: DOI 10.1021/ic00121a013.

(36) Noodleman, L.; Case, D. A.; Aizman, A. Broken Symmetry Analysis of Spin Coupling in Iron Sulfur Clusters. *J. Am. Chem. Soc.* **1988**, *110*, 1001-1005. DOI: DOI 10.1021/ja00212a003.

(37) Neese, F. The ORCA Program System. *Wiley Interdisciplinary Reviews-Computational Molecular Science* **2012**, *2*, 73-78. DOI: Doi 10.1002/Wcms.81.

(38) Neese, F. Software Update: The Orca Program System—Version 5.0. *WIREs Computational Molecular Science* **2022**, *12*, e1606. DOI: https://doi.org/10.1002/wcms.1606.

(39) Jodts, R. J.; Wittkop, M.; Ho, M. B.; Broderick, W. E.; Broderick, J. B.; Hoffman, B. M.; Mosquera, M. A. Computational Description of Alkylated Iron-Sulfur Organometallic Clusters. *J. Am. Chem. Soc.* **2023**, *145*, 13879-13887. DOI: 10.1021/jacs.3c03062.

(40) Becke, A. D. A New Mixing of Hartree–Fock and Local Density-Functional Theories. *J. Chem. Phys.* **1993**, *98*, 1372-1377. DOI: 10.1063/1.464304.

(41) Barone, V.; Bencini, A.; Ciofini, I.; Daul, C. A.; Totti, F. Density Functional Modeling of Couble Exchange Interactions in Transition Metal Complexes. Calculation of the Ground and Excited State Properties of $[Fe_2(OH)_3(Tmtacn)_2]^{2+}$. *J. Am. Chem. Soc.* **1998**, *120*, 8357-8365.

(42) Schafer, A.; Horn, H.; Ahlrichs, R. Fully Optimized Contracted Gaussian-Basis Sets for Atoms Li to Kr. *J. Chem. Phys.* **1992**, *97*, 2571-2577.

(43) Neese, F. Prediction and Interpretation of the ^{57}Fe Isomer Shift in Mössbauer Spectra by Density Functional Theory. *Inorg. Chim. Acta* **2002**, *337*, 181-192. DOI: https://doi.org/10.1016/S0020-1693(02)01031-9.

(44) McConnell, H. M.; Robertson, R. E. Spectroscopic Splitting Factors in Aromatic Radicals. *J. Phys. Chem.* **1957**, *61*, 1018.

(45) Box, H. C.: *Radiation Effects: ESR and ENDOR Analysis*; Academic Press: New York, 1977.

(46) Schweiger, A.; Jeschke, G.: *Principles of Pulse Electron Paramagnetic Resonance*; Oxford University Press: Oxford, UK, 2001.

(47) Werst, M. M.; Kennedy, M. C.; Houseman, A. L.; Beinert, H.; Hoffman, B. M. Characterization of the $[4Fe\text{-}4S]^+$ Cluster at the Active Site of Aconitase by ^{57}Fe, ^{33}S, and ^{14}N Electron Nuclear Double Resonance Spectroscopy. *Biochemistry* **1990**, *29*, 10533-10540. DOI: 10.1021/bi00498a016.

(48) Kappl, R.; Ciurli, S.; Luchinat, C.; Huttermann, J. Probing Structural and Electronic Properties of the Oxidized $[Fe_4S_4]^{3+}$ Cluster of Ectothiorhodospira Halophila Iso-II High-Potential Iron-Sulfur Protein by Endor Spectroscopy. *J. Am. Chem. Soc.* **1999**, *121*, 1925-1935.

(49) Carrington, A.; McLachlan, A. D.: *Introduction to Magnetic Resonance with Applications to Chemistry and Chemical Physics*; Harper & Row: New York, 1967.

(50) Schatz, G. C.; Ratner, M. A.: *Quantum Mechanics in Chemistry*; Prentice Hall: Englewood Cliffs, N.J., 1993.

(51) Adrian, F. J. Matrix Effects on the Electron Spin Resonance Spectra of Trapped Hydrogen Atoms. *J. Chem. Phys.* **1960**, *32*, 972-981. DOI: 10.1063/1.1730906.

(52) Horitani, M.; Offenbacher, A. R.; Carr, C. A.; Yu, T.; Hoeke, V.; Cutsail, G. E., 3rd; Hammes-Schiffer, S.; Klinman, J. P.; Hoffman, B. M. ^{13}C ENDOR Spectroscopy of Lipoxygenase-Substrate Complexes Reveals the Structural Basis for C-H Activation by Tunneling. *J. Am. Chem. Soc.* **2017**, *139*, 1984-1997. DOI: 10.1021/jacs.6b11856.

(53) Vey, J. L.; Yang, J.; Li, M.; Broderick, W. E.; Broderick, J. B.; Drennan, C. L. Structural Basis for Glycyl Radical Formation by Pyruvate Formate-Lyase Activating Enzyme. *PNAS* **2008**, *105*, 16137-16141. DOI: 10.1073/pnas.0806640105.

(54) Moody, J. D.; Hill, S.; Lundahl, M. N.; Saxton, A. J.; Galambas, A.; Broderick, W. E.; Lawrence, C. M.; Broderick, J. B. Computational Engineering of Previously Crystallized Pyruvate Formate-Lyase Activating Enzyme Reveals Insights into SAM Binding and Reductive Cleavage. *J. Biol. Chem.* **2023**, *299*, 104791. DOI: 10.1016/j.jbc.2023.104791.

(55) PyMOL; ed. 2.3.5; Schrödinger, LLC; New York, NY; 2019

(56) Cosper, N. J.; Booker, S. J.; Ruzicka, F.; Frey, P. A.; Scott, R. A. Direct FeS Cluster Involvement in Generation of a Radical in Lysine 2,3-Aminomutase. *Biochemistry* **2000**, *39*, 15668-15673.

(57) Chen, D.; Walsby, C.; Hoffman, B. M.; Frey, P. A. Coordination and Mechanism of Reversible Cleavage of S-Adenosylmethionine by the [4Fe-4S] Center in Lysine 2,3-Aminomutase. *J. Am. Chem. Soc.* **2003**, *125*, 11788-11789.

(58) Wang, S. C.; Frey, P. A. Binding Energy in the One-Electron Reductive Cleavage of S-Adenosylmethionine in Lysine 2,3-Aminomutase, a Radical SAM Enzyme. *Biochemistry* **2007**, *46*, 12889-12895. DOI: 10.1021/bi701745h.

TOC:

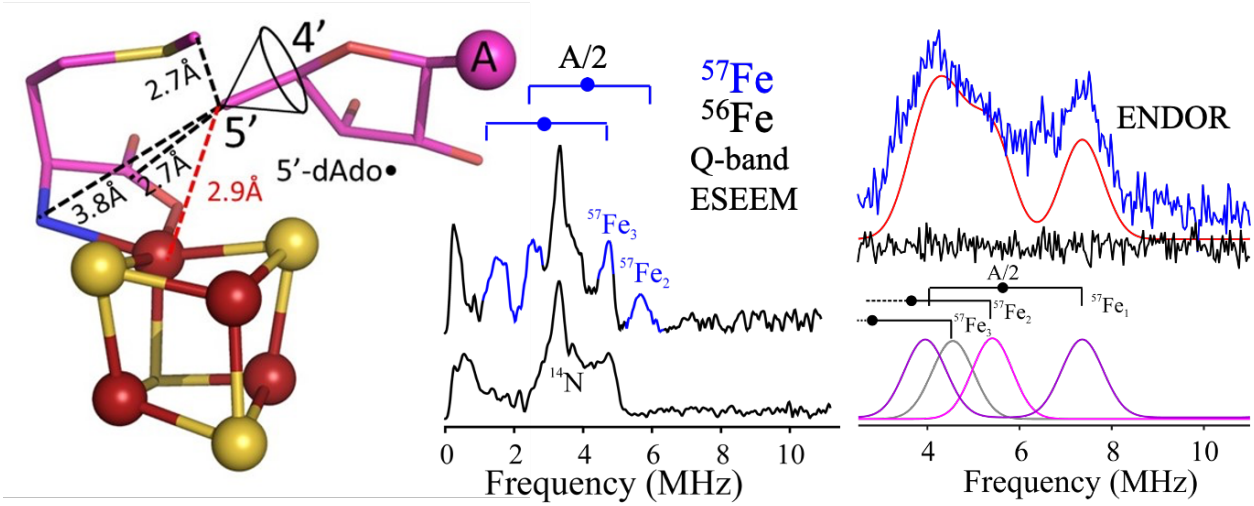
4'
A
2.7Å
5'
2.7Å
3.8Å
2.9Å
5'-dAdo•
A/2
57Fe
56Fe
Q-band
ESEEM
57Fe3
57Fe2
14N
0
2
4
6
8
10
Frequency (MHz)
ENDOR
A/2
57Fe1
57Fe2
57Fe3
4
6
8
10
Frequency (MHz)